The California Current System during the last 136,000 years: Response of the North Pacific High to precessional forcing

Masanobu Yamamoto[1*], Masumi Yamamuro[2] and Yuichiro Tanaka[2]

[1]*Faculty of Environmental Earth Science, Hokkaido University, Sapporo 060-0810, Japan*

[2]*Geological Survey of Japan, AIST, Tsukuba, Ibaraki 305-8567, Japan*

*Corresponding author; Phone/Fax: +81-11-706-2379, E-mail: myama@ees.hokudai.ac.jp (M. Yamamoto)

Abstract

Alkenone sea surface temperature (SST) records were generated from the Ocean Drilling Program's (ODP) Sites 1014 and 1016 to examine the response of the California Current System to global climate change during the last 136 kyr. The temperature differences between these sites ($\Delta SST_{NEP} = SST_{ODP1014} - SST_{ODP1016}$) reflected the intensity of the California Current and varied between 0.4˚ and 6.1˚C. A high ΔSST_{NEP} (weaker California Current) was found for late MIS (marine isotope stage) 2 and early MIS 5e, while a low ΔSST_{NEP} (stronger California Current) was detected for mid-MIS 5e and MIS 1. Spectral analysis indicated that this variation pattern dominated 23-kyr (precession) and 30-kyr periods. Comparison of the ΔSST_{NEP} and SST based on data from core MD01-2421 at the Japan margin revealed anti-phase variation; the high ΔSST_{NEP} (weakening of the California Current) corresponded to the

low SST at the Japan margin (the southward displacement of the NW Pacific subarctic boundary), and vice versa. This variation was synchronous with a model prediction of the tropical El Niño–Southern Oscillation behavior. These findings suggest that the intensity of the North Pacific High varied in response to precessional forcing, and also that the response has been linked with the changes of tropical ocean-atmosphere interactions.

1. Introduction

The California Current System (CCS) is an eastern boundary current system in the North Pacific that consists of the southward California Current, northward Southern California Countercurrent, Davidson Current and California Undercurrent, as shown in Fig. 1 (Hickey, 1979). Previous studies finding decreased productivity (Lyle et al., 1992) and an increased meridional paleo-SST gradient (Doose et al., 1997; Mangelsdorf et al., 2000; Herbert et al., 2001) have suggested that the California Current declined during the last glacial maximum. This decline has been attributed to the depressed summer North Pacific High influenced by the semipermanent development of a high-pressure cell over the expanded Laurentide ice sheet on the North American continent (Kutzbach and Wright, 1985; Lyle et al., 1992). Recently, Yamamoto et al. (2004) noted that SST variation at the California margin did not fully agree with the development of the Laurentide ice sheet but did correspond to SSTs at the Japan margin, suggesting basin-scale variation in North Pacific SSTs.

The relative intensities of the California Current and the Southern California Countercurrent are controlled by the development of the North Pacific High (Hickey, 1979). California Current water originates from the subarctic West Wind Drift and the

subtropical North Pacific Current (Hickey, 1979). Subarctic water contributions and the intensity of the California Current increase during summer due to a strengthened North Pacific High (Hickey, 1979). The Southern California Countercurrent is a northward flow that occurs during most of the year except for spring; the countercurrent becomes seasonally intensified in late fall and winter (Hickey, 1979) and annually in El Niño years due to the weaker North Pacific High (Bograd and Lynn, 2001).

In this study, we compared alkenone-derived SST records at ODP Sites 1014 and 1016 to clarify the response of the CCS to global climate change during the last 136 kyr. Sites 1014 and 1016 were drilled during ODP Leg 167 in 1996 (Lyle et al., 1997). Site 1014 is influenced by the northward invasion of the Southern California Countercurrent into the California Borderland region. Site 1016 is located along the main path of the California Current. The temperature difference between these sites must therefore reflect the relative intensities of the California Current and the Southern California Countercurrent.

Paleo-SSTs during the last glacial maximum (LGM) were estimated using alkenones, foraminifers, radiolarians and pollen at numerous locations along the California margin. Along the northern and central California margin, alkenone-derived temperatures (Prahl et al., 1995; Doose et al., 1997; Mangelsdorf et al., 2000; Seki et al., 2002) agreed with those estimated using radiolarian assemblages (Sabin and Pisias, 1996) and foraminiferal $\delta^{18}O$ and their assemblages (Ortiz et al., 1997); these data indicate that temperatures were ~4°C lower in the LGM than in the Holocene. In contrast, at the southern California margin (the California Borderland), alkenone-derived temperatures disagreed with foraminiferal and pollen-derived temperatures during the LGM. Alkenone temperature estimations have indicated that the LGM was 0°–2°C cooler than

the Holocene (Herbert et al., 1995; Doose et al., 1997; Hinrichs et al., 1997), whereas temperature estimations using the sinistral/dextral ratios of *Neogloboquadrina pachyderma*, $\delta^{18}O$ of planktonic foraminifers, and foraminiferal assemblages have indicated that the LGM was more than 5°C cooler than the Holocene (Kahn et al., 1981; Kennett and Ingram, 1995; Kennett and Venz, 1995; Thunell and Mortyn, 1995; Mortyn et al., 1996). Pollen assemblages at Site 893 agreed with foraminiferal SST estimations (Heusser, 1995). This "temperature disagreement" in the California Borderland remains an open question. We examined this issue by comparing variations in the unsaturation parameters of alkenones and alkenoates with planktonic foraminiferal $\delta^{18}O$.

2. Materials and methods

Cores 167-1014A-1H, 2H and 3H (ODP Site 1014; 0–16.9 m below the sea floor [mbsf]) were collected in the Tanner Basin (32°48'N, 118°54'W) at a water depth of 1165 m (Lyle et al., 1997; Fig. 1). The sediment cores consisted of dark olive gray to dark gray hemipelagic clay interbedded nannofossil ooze containing foraminifers throughout (Lyle et al., 1997). Samples of approximately 10 cm^3 in volume were taken every 20 cm and immediately frozen in N_2-filled Kapack bags. The age model (Table 1 and Fig. 2) was created by oxygen isotope stratigraphy (Martinson et al., 1987) of the benthic foraminifera *Uvigerina* (Hendy and Kennett, 2000) and by calendar ages converted from the AMS ^{14}C ages of seven bulk organic matter samples (2.30–20.55 ka). The ^{14}C ages were converted to calendar ages using the CALIB4.3 marine98 program (Stuiver and Reimer, 1993) and an equation by Bard (1998) with a 633-year reservoir correction for the California margin (Ingram and Southon, 1996).

Core 167-1016C-1H (ODP Site 1016; 0–9.2 mbsf) was collected off the coast of

central California (34°32'N, 122°17'W) at 3834 m water depth (Lyle et al., 1997; Fig. 1). Core sediments consisted of gradationally interbedded dark gray to dark greenish gray diatom ooze and light greenish yellow to light olive gray diatom nannofossil ooze (Lyle et al., 1997). The core was sealed in a N_2-filled oxygen-impermeable plastic bag immediately after recovery and stored in a refrigerator for three months until shore-based sampling. Samples of approximately 10 cm^3 in volume were taken every 9 cm and immediately frozen. The age model was created with calendar ages converted from the AMS ^{14}C ages of eleven bulk organic matter samples (5.66–37.72 ka) using the same program and reservoir correction method as for cores 167-1014A (Table 2 and Fig. 2). Correlating the $\delta^{15}N$ values of this core with those of Site 1014 established that the age–depth model extended to 135.57 ka, as described in Section 3.1.

Alkenones and alkenoates were analyzed following the method of Yamamoto et al. (2000). The separation of all alkenones and alkenoates was enough for accurate quantification (Fig. 7 in Yamamoto et al., 2000). The alkenone unsaturation index $U^{K'}_{37}$ was calculated from the concentrations of di- and tri-unsaturated C_{37} alken-2-ones [C_{37}MK] using the following expression (Prahl et al., 1988):

$$U^{K'}_{37} = [C_{37:2}MK]/([C_{37:2}MK] + [C_{37:3}MK]).$$

Temperature was calculated according to the equation

$$U^{K'}_{37} = 0.034T + 0.039,$$

where T = temperature [°C]) based on experimental results for cultured strain 55a of

Emiliania huxleyi (Prahl et al., 1988); analytical accuracy was 0.24°C in our laboratory. The culture-based calibration (Prahl et al., 1988) was nearly identical to the core-top calibration along the California margin (Herbert et al., 1998). Additional unsaturation indices for U^{me}_{36} and $K_{37:4}/K_{37}$ were calculated using the following equations (Prahl et al., 1995):

$$U^{me}_{36} = [C_{36:2}ME]/([C_{36:2}ME] + [C_{36:3}ME]),$$

where $[C_{36}ME]$ is the concentration of C_{36} fatty acid-methyl ester, and

$$K_{37:4}/K_{37} = [C_{37:4}MK]/([C_{37:2}MK] + [C_{37:3}MK] + [C_{37:4}MK]).$$

To determine stable nitrogen isotope ratios, samples were combusted at 1020°C in a Fisons Instruments EA1108 elemental analyzer (Beverly, MA, USA). The generated N_2 was introduced into a Finnigan Delta Plus isotope-ratio mass spectrometer (Thermo Electron Corp., Waltham, MA, USA) by using a He carrier. The ratio of $^{15}N/^{14}N$ was expressed relative to the N_2 in air. Machine drift during analyses was checked with l-α-alanine ($\delta^{15}N$ = 7.61‰) every three samples. Accuracy was determined using interlaboratory-determined nitroarginine following the method of Minagawa et al. (1984).

We performed spectral analyses using the Blackman–Tuckey and Cross–Blackman–Tuckey methods provided in the Analyseries software package (Paillard et al., 1996).

3. Results and discussion

3.1. Nitrogen isotopes and the age–depth model of Site 1016

Oxygen isotope stratigraphy could not be used to establish the age–depth model of Site 1016 because carbonates had dissolved at most intervals. Instead, we established that the age–depth model extended to 135.57 ka (Table 2 and Fig. 2) by correlating $\delta^{15}N$ values of this core with those of Site 1014 (Fig. 3). Because the $\delta^{15}N$ values of cores in the Northeastern Pacific rim from the Mexico to Oregon margins varied synchronously during the last glacial age (Kienast et al., 2002), $\delta^{15}N$ could be used for stratigraphic correlation for the California margin. The $\delta^{15}N$ values ranged from ~5 to 9 ‰ (Fig. 3); this variation was synchronous with that in the Mexican margin (Ganeshram et al., 1995) except that the $\delta^{15}N$ maximum for MIS 5a was more enhanced for Sites 1014 and 1016 than that at the Mexican margin. The $\delta^{15}N$ values were generally 0–2 ‰ higher for the deeper site (Site 1016) than the shallower site (Site 1014). This difference was consistent with the observation that the isotopic fractionation of $\delta^{15}N$ between sinking particles and surface sediments tends to increase with increasing water bottom depth (Nakanishi and Minagawa, 2003).

3.2. Paleo-SSTs at the California margin

At Site 1014, SSTs ranged from 12˚ to 19˚C during the last 158 ka, whereas at Site 1016, SSTs ranged from 9˚ to 18˚C during the last 136 ka (Fig. 3). The core-top temperatures of Sites 1014 and 1016 were ~16°C and ~14°C, respectively, in agreement with present annual mean SSTs at these sites (Robinson, 1976). This result is concordant with the observation that core-top $U^{K'}_{37}$-derived temperatures represent the

annual mean SSTs along the California margin (Herbert et al., 1998). At both sites, the SST increase preceded the MIS 1/2 and 5/6 boundaries by ~8 and ~6 kyr, respectively (Fig. 3). This early warming was more evident at Site 1014 than at Site 1016 (Fig. 3), implying a stronger Southern California Countercurrent (Herbert et al., 2001) analogous to a modern El Niño condition (Bograd and Lynn, 2001) at the latest glacial stage. Strong cooling was observed around the MIS 2/3 and 3/4 boundaries (Fig. 3). *Coccolithus pelagicus*, a coccolithophore specific to subarctic waters in the North Pacific (Okada and McIntyre, 1977), was abundant during the same intervals at Site 1014 (Fig. 4; Tanaka, Y., unpublished data). These observations indicate an intensified California Current analogous to a modern La Niña condition during those periods.

In the Tanner Basin, the $U^{K'}_{37}$-derived paleo-temperatures during the latter half of MIS 2 at Site 1014 were more than 4°C higher than those indicated by foraminiferal $\delta^{18}O$ and assemblages in core AHF10164 (Kahn et al., 1981). Interestingly, the U^{me}_{36} and $K_{37:4}/K_{37}$ profiles were similar to the $\delta^{18}O$ profile of planktonic foraminifera *Globigerina bulloides* around MIS 2 (Hendy and Kennett, 2000) but differed from the $U^{K'}_{37}$ profile at Site 1014 (Fig. 4). However, the U^{me}_{36} and $K_{37:4}/K_{37}$ profiles were similar to the $U^{K'}_{37}$ profile at Site 1016 (Yamamoto et al., 2000; Fig. 4). The $U^{K'}_{37}$ profile showed good correlation with U^{me}_{36} and $K_{37:4}/K_{37}$ at Site 1016; however, $U^{K'}_{37}$ values from late MIS 2 samples were higher than those of other intervals at Site 1014 (Fig. 5). This finding suggests multiple sources of alkenones and alkenonates at Site 1014 in late MIS 2. At least two major sources are indicated. The first source may have been C_{36}ME- and $C_{37:4}$MK-rich species that bloomed in cooler water. The second source may have been C_{36}ME- and $C_{37:4}$MK-poor species that bloomed in warmer water. Sediment-trap studies at the Santa Barbara Basin demonstrated that when the spring

upwelling was reduced under El Niño conditions, coccolithophore export production was enhanced particularly for the tropical species *Gephyrocapsa oceanica* (De Bernardi et al., 2005), while the export production of the planktonic foraminifers *Globigerina bulloides* and *Neogloboquadrina pachyderma* (dextral) was reduced (Pak et al., 2004). Frequent invasions of subtropical water to the California Borderland during late MIS 2, which was analogous to modern El Niño conditions (Bograd and Lynn, 2001), may therefore have enhanced haptophyte blooms possibly by the second type of alkenone producer noted above and reduced the blooms of planktonic formaninifers and the first type of alkenone producer. This ecological setting possibly caused the $U^{K'}_{37}$ to record warmer temperatures than those by foraminifers and U^{me}_{36}. The high $U^{K'}_{37}$ during late MIS 2 might more accurately reflect the frequent invasion of warmer water to the California Borderland.

3.3. Variations of the CCS on orbital timescales

Site 1014 experiences the northward invasion of the Southern California Countercurrent to the California Borderland, while Site 1016 is located along the main path of the California Current. Thus, the temperature difference between these sites reflects the relative intensities of the California Current and the Southern California Countercurrent. We obtained SST differences for the Sites 1014 and 1016 (ΔSST_{NEP}) for the last 136 kyr by subtracting the SST of Site 1016 from that of Site 1014 (Fig. 3). The ΔSST_{NEP} varied between 0.4˚ and 6.1˚C with an average of 2.9˚C. A high ΔSST_{NEP} (weaker California Current) was observed in late MIS 2 and early MIS 5e, while a low ΔSST_{NEP} (stronger California Current) was observed in mid-MIS 5e and MIS 1.

We evaluated the effects of time-scale uncertainty on the ΔSST_{NEP} profile by

comparing various ΔSST_{NEP} profiles obtained under the assumption that the ages of Site 1016 shift in the direction of younger or older. Because the sample intervals of $\delta^{15}N$ measurement were ~1.3 kyr at Site 1016, the maximum error in the direct correlation of $\delta^{15}N$ must be ~1.3 kyr, although errors caused by other factors were not evaluated in detail. Shifting the ages of Site 1016 to younger and older directions within 3 kyr did not change the ΔSST_{NEP} profile, which shows high ΔSST_{NEP} in late MIS 2, mid-MIS 3, MIS 5a and early MIS 5e and low ΔSST_{NEP} in MIS 1, early MIS 3, the MIS 4/5a boundary and MIS 5b. One exception was mid-MIS 5e. Shifting to the younger direction by 1-3 kyr weakened the negative peak at mid-MIS 5e.

Previous studies have suggested a decline in the California Current during MIS 2 based on decreased productivity (Lyle et al., 1992) and an increased meridional paleo-SST gradient (Doose et al., 1997; Mangelsdorf et al., 2000). Herbert et al. (2001) showed that an early warming at the California Borderland began ~24 ka, and the SST reached a maximum value at ~16 ka (late MIS 2), reflecting weakening of the California Current. This decline was attributed to a depressed summer North Pacific High influenced by the semipermanent development of a high-pressure cell over the expanded Laurentide ice sheet over continental North America (Kutzbach and Wright, 1985; Lyle et al., 1992). However, paleo-SST change at Site 1014 did not fully agree with the estimated volume change of the Laurentide ice sheet (Boulton et al., 1985). In particular, a low SST and abundant *C. pelagicus* indicate a strong California Current in late MIS 4; however, the second-largest expanse of the Laurentide ice sheet during the last glacial period also occurred during this time (Fig. 4). Thus, the volume of the Laurentide ice sheet may not have been the only factor affecting the CCS.

Spectral analyses indicated that the SST variation patterns of Sites 1014 and 1016

dominate 100-kyr (eccentricity), 41-kyr (obliquity), and 23-kyr (precession) periods and are highly coherent at these frequencies with the $\delta^{18}O$ variation of the benthic foraminifera *Uvigerina* at Site 1014 (Fig. 6A and 6B). However, the variation pattern of ΔSST_{NEP} dominated 23-kyr and 30-kyr periods (Fig. 6C).

Comparing the ΔSST_{NEP} and the SST of MD01-2421 at the Japan margin revealed an anti-phase variation during the last 136 kyr (Fig. 7). Both ΔSST_{NEP} and the SST of MD01-2421 showed variations in 23-kyr and 30-kyr periods and lacked a 41-kyr period (Fig. 6C and 6D). Cross-spectral analysis indicated that ΔSST_{NEP} variation is highly coherent with the SST variation of MD01-2421 at 23-kyr and 30-kyr periods, and also indicated that the ΔSST_{NEP} led the SST of MD01-2421 by 169±12 and 127±11° at 23-kyr and 30-kyr bands, respectively. The high ΔSST_{NEP} at the California margin corresponded to the low SST at the Japan margin, and vice versa (Fig. 7).

At the Japan margin, the alkenone SST variation mainly reflects the latitudinal displacement of the subarctic boundary in summer (Yamamoto et al., 2004, 2005). The latitudinal position of the subarctic boundary associated with the westerly jet in summer is principally controlled by the relative intensities of the North Pacific High and the Okhotsk High (Nitta, 1987; Goes et al., 2001). A low SST reflects the southward displacement of the subarctic boundary, resulting from the weaker North Pacific High. The observed SST of alkenone maximum production season (July and August) at the site of MD01-2421 from 1950 to 2002 has positive correlation ($r = 0.39$, $n = 53$, $p < 0.05$) with the intensity of the summer North Pacific High (Isono and Yamamoto, unpublished data). Thus, the high ΔSST_{NEP} at the California margin and the low SST at the Japan margin both resulted from a weaker North Pacific High, and vice versa. The

anti-phase relationship between ΔSST_{NEP} and the SST of MD01-2421 at the precession band suggests that variation in the CCS at 23-kyr periods is a part of the response of the North Pacific High to precessional forcing.

A 30-kyr period was previously reported in the variations of atmospheric carbon dioxide concentration recorded in the Vostok ice core (Petit et al., 1999) and in the paleo-productivity records in the tropical Indo-Pacific (e.g., Beaufort et al., 2001; 2003). At the 30-kyr band, the ΔSST_{NEP} maxima (the weakest California Current) lagged the CO_2 concentration minima by 11±15°, and the SST maxima of MD01-2421 lagged the CO_2 concentration maxima by 39±23° (Fig. 8). The phase lag between the ΔSST_{NEP} maxima and the SST maxima of MD01-2421 was 127±11°; the relationship was not anti-phase. This phase lag suggests that these variations were not a simple result of the response of the North Pacific High, but were interfered by an unknown factor at either the California or Japan margin.

3.4. Linkage between the CCS and tropical Indo-Pacific climates

Both the ΔSST_{NEP} and SST at the Japan margin are controlled by the intensity of the North Pacific High. The North Pacific High is influenced by modern interannual El Niño-Southern Oscillation (ENSO) through atmospheric teleconnections (Bograd and Lynn, 2001). In El Niño years, the tropical convection center moves to the central and eastern equatorial Pacific. This process weakens the North Pacific High in summer, resulting in a warming of the California Borderland by the intensification of the Southern California Countercurrent (Bograd and Lynn, 2001). At the Japan margin, the depressed North Pacific High in the summer of El Niño years tend to delay the northward shifts of the westerly jet and oceanic subarctic boundary (Goes et al., 2001)

and thus cool the Japan margin in summer (Nitta, 1987; Kawamura et al., 1998). In La Niña years, the tropical convection center moves to the western equatorial Pacific, intensifying the summer North Pacific High and the California Current and cooling the California margin. This process excites the Pacific–Japan teleconnection pattern in summer (Nitta, 1987) and accelerates the northward shift of the subarctic boundary, warming the Japan margin (Nitta, 1987; Kawamura et al., 1998).

Zebiak-Cane ENSO model calculations for the past 150 kyr demonstrated that seasonal anomalies in insolation driven by precession could have changed ENSO behaviors (see the calculated NINO3 in Fig. 7; Clement et al., 1999). In the modern Pacific, the Intertropical Convergence Zone (ITCZ) nears the equator in spring, generating a zonal symmetric response in atmospheric heating, while the eastern Pacific ITCZ moves north in autumn, generating zonal asymmetry in atmospheric heating. The model calculation assumes that when the perihelion occurs in spring, uniform atmospheric heating of the tropical Pacific generates a background state giving an El Niño-like response; for an autumn perihelion, asymmetric atmospheric heating generates a background state creating a La Niña-like response.

Beaufort et al. (2001) generated late Pleistocene sediment records of nannofossil-derived paleo-productivity along the equator in the Indian and Pacific oceans. Their study showed that variations in equatorial productivity have been caused primarily by both glacial-interglacial variability and precession-controlled changes in the east-west thermocline slope of the Indo-Pacific. Precession-controlled variations in productivity were linked to processes similar to the ENSO phenomenon and preceded changes in the $\delta^{18}O$ of benthic foraminifera (Fig. 8), indicating that these changes did not result from ice sheet fluctuations.

At the precession band, the intensity minima of the North Pacific High was in phase with the April perihelion and the maxima of predicted NINO3 index (Clement et al., 1999; Fig. 8). However, productivity variation in the tropical Indo-Pacific (Beaufort et al., 2001) was out of phase with the ΔSST_{NEP} and the predicted NINO3 (Fig. 8). The El Niño-like phase of the thermocline slope lagged the ΔSST_{NEP} maxima and the predicted NINO3 maxima by ~120° (Fig. 8). Our results and those of the model prediction indicate that the weakest North Pacific High and the optimal phase of the El Niño-like condition lagged the ice volume maxima, while the productivity records (Beaufort et al., 1999) indicate that the optimal El Niño-like phase preceded the ice volume minima (Fig. 8). This phase discrepancy of long-term ENSO-like variability remains a key question because little is known about the behavior of tropical ocean-atmosphere interactions at orbital timescales, although shorter paleo-records in the eastern tropical Pacific and the tropical Andes regions were consistent with the model prediction (e.g., Koutavas et al., 2002; Moy et al., 2002).

The precession wheel in Fig. 8 illustrates that the strongest North Pacific High (ΔSST_{NEP} minima) led by ~30° (~2 kyr) with the maxima of the Indian summer monsoon (based on the summer monsoon stack by Clemens and Prell, 2003) and East Asian summer monsoon (based on the abundance of a Japanese cedar [*Cryptomeria japonica*] pollen in the NW Pacific off Japan by Morley and Heusser, 1997; Igarashi and Oba, 2006). Meteorological studies demonstrated a close linkage between boreal summer monsoon (BSM) and ENSO; the stronger BSM corresponds to the La Niña state of the tropical Pacific, and the weaker BSM corresponds to the El Niño state (e.g., Meehl, 1987; Yasunari, 1991). Heusser and Sirocko (1997) reported a large centennial-scale fluctuation of pollen assemblages during the last deglaciation in ODP

Site 893, Santa Barbara Basin, California margin. They suggested that correlative high-frequency variations for the northeast Pacific winter and southern Asian summer climates may reflect submillennial-scale ENSO-type forcing involving water vapor transport over the Indian and Pacific oceans. Theses modern and centennial-scale studies suggest the synchronous climate variations throughout the Indo-Pacific region. In contrast, our orbital-timescale records demonstrated the phase lead of the North Pacific High to boreal monsoon variations, suggesting either that the ENSO-like variability has been independent of BSM or that the ENSO-like variability has caused the change of BSM.

4. Conclusion

The present study presents the new perspective that variation of the CCS is part of a basin-scale oceanic and atmospheric response in the North Pacific. The variation indicates that the North Pacific High varied in response to precessional forcing. Long-term ENSO-like variability and wave propagation by teleconnection (Heusser and Sirocko, 1997; Clement et al., 1999; Beaufort et al., 2001; Yamamoto et al., 2004) are potential driving forces of the basin-scale climate response. Establishing the linkage between this basin-scale response and tropical ocean-atmospheric dynamics will be a key toward better understanding the role of the Indo-Pacific in global climate change.

Acknowledgements We thank Kazuko Hino for analytical assistance in the laboratory. Special thanks are due to Ryuji Tada, Itaru Koizumi, Tomohisa Irino, Yaeko Igarashi, Tadamichi Oba, and Masatoshi Komiya, for valuable discussions. We also thank Timothy D. Herbert for his helpful comments in review and Peter Clark for his editorial

handling. This research used samples and data provided by the Ocean Drilling Program (ODP). The ODP is sponsored by the U.S. National Science Foundation (NSF) and participating countries under management of Joint Oceanographic Institution (JOI), Inc. This study was supported by financial aid from the Science and Technology Agency of Japan.

References

Bard, E., 1998. Geochemical and geophysical implications of radiocarbon calibration. Geochim. Cosmochim. Acta 62, 2025-2038.

Beaufort, L., de Garidel-Thoron, T., Mix, A.C., Pisias, N.G., 2001. ENSO-like forcing on oceanic primary production during the late Pleistocene. Science 293, 2440-2444.

Beaufort, L., de Garidel-Thoron, T., Linsley, B., Oppo, D., Buchet, N., 2003. Biomass burning and ocean primary production estimates in the Sulu Sea over the last 380 kyr and the East Asian monsoon dynamics. Mar. Geol. 201, 53-65.

Bograd, S., Lynn, R.J., 2001. Physical-biological coupling in the California Current during the 1997-99 El Niño-La Niña cycle. Geophys. Res. Let. 28, 275-278.

Boulton, G.S., Smith, G.D., Jones, A.S., Newsome, J., 1985. Glacial geology and glaciology of the last mid-latitude ice sheets. J. Geol. Soc. (London) 142, 447-474.

Clemens, S.C., Prell, W.L., 2003. A 350,000 year summer-monsoon multi-proxy stack from the Owen Ridge, Northern Arabian Sea. Marine Geology 201, 35-51.

Clement, A.C., Seager, R., Cane, M.A., 1999. Orbital controls on the El Niño/Southern Oscillation and the tropical climate. Paleoceanogr. 14, 441-456.

De Bernardi, B., Ziveri, P., Erba, E., Thunell, R.C., 2005. Coccolithophore export production during the 1997-1998 El Niño event in Santa Barbara basin (California).

Mar. Micropaleontol. 55, 107-125.

Doose, H., Prahl, F.G., Lyle, M.W., 1997. Biomarker temperature estimates for modern and last glacial surface waters of the California Current system between 33° and 42°N. Paleoceanogr. 12, 615-622.

Ganeshram, R.S., Pedersen, T.F., Calvert, S.E., Murray, J.W., 1995. Large changes in oceanic nutrient inventories from glacial to interglacial periods. Nature 376, 755-757.

Goes, J.I., Gomes, H.R., Limsakul, A., Balch, W.M., Saino, T., 2001. El Niño related interannual variations in biological production in the North Pacific as evidenced by satellite and ship data. Prog. Oceanogr. 49, 211-225.

Hendy, I.L., Kennett, J.P., 2000. Stable isotope stratigraphy and paleoceanography of the last 170 ka: ODP Site 1014, Tanner Basin, California. Proc. ODP Sci. Res. 167, 129-140.

Herbert, T.D., Yasuda, M., Burnett, C., 1995. Glacial-interglacial sea-surface temperature record inferred from alkenone unsaturation indices, Site 898, Santa Barbara basin. Proc. ODP, Sci. Res. 146, 257-263.

Herbert, T.D., Schuffert, J.D., Thomas, D., Lange, C., Weinheimer, A., Peleo-Alampay, A., Herguera, J.-C., 1998. Depth and seasonality of alkenone production along the California margin inferred from a core top transect. Paleoceanogr. 13, 263-271.

Herbert, T.D., Schuffert, J.D., Andreasen, D., Heusser, L., Lyle, M., Mix, A., Ravelo, A.C., Stott, L.D., Herguera, J.C., 2001. Collapse of the California Current during glacial maxima linked to climate change on land. Science 293, 71-76.

Heusser, L.E., 1995. Pollen stratigraphy and paleoecologic interpretation of the 160-K.Y. record from Santa Barbara Basin, Hole 893A. Proc. ODP Sci. Res. 146, 265-279.

Heusser, L.E., Sirocko, F., 1997. Millennial pulsing of environmental changes in southern California from the past 24 k.y.: A record of Indo-Pacific ENSO events? Geology 25, 243-246.

Hickey, B.M., 1979. The California Current System-hypotheses and facts. Prog. Oceanog. 8, 191-279.

Hinrichs, K.-U., Rinna, J., Rullkötter, J., Stein, R., 1997. A 160 kyr record of alkenone-derived sea-surface temperatures from Santa Barbara basin sediments. Naturwissenschaften 84, 126-128.

Igarashi, Y., Oba, T., 2006. Fluctuations of monsoons and insolation in the northwest Pacific during the last 144 kyr from a high-resolution pollen analysis of the IMAGES core MD01-2421. Quat. Sci. Rev., 25, 1447-1459. doi:10.1016/j.quascirev.2005.11.011

Imbrie, J., et al., 1984. The orbital theory of Pleistocene climate: support from a revised chronology of the marine $\delta^{18}O$ record. In: Berger, A.L., et al. (Ed.), Milankovitch and Climate. Part I. D. Reidel, Dordrecht. pp. 269-305.

Ingram, B.L., Southon, J.R., 1996. Reservoir ages in eastern Pacific coastal and estuarine waters. Radiocarbon 38, 573-582.

Kahn, M.I., Oba, T., Ku, T.-L., 1981. Paleotemperatures and the glacially induced changes in the oxygen-isotope composition of sea water during late Pleistocene and Holocene time in Tanner Basin, California. Geology 9, 485-490.

Kawamura, R., Sugi, M., Kayahara, T., Sato, N., 1998. Recent extraordinary cool and hot summers in East Asia simulated by an ensemble climate experiment. J. Metor. Soc. Japan 76, 597-617.

Kennett, J.P., Ingram, B.L., 1995. A 20,000-year record of ocean circulation and climate

change from the Santa Barbara basin. Nature 377, 510-512.

Kennett, J.P., Venz, K., 1995. Late Quaternary climatically related planktonic foraminiferal assemblage changes: Hole 893A, Santa Barbara Basin, California. Proc. ODP Sci. Res. 146, 281-293.

Kienast, S.S., Calvert, S.E., Pedersen, T.F., 2002. Nitrogen isotope and productivity variations along the northeast Pacific margin over the last 120 kyr: Surface and subsurface paleoceanography. Paleoceanogr. 17, 1055, doi: 10.1029/2001PA000650.

Koutavas, A., Lynch-Stiegletz, J., Marchitto, T.M., Sachs, J., 2002. El Niño-like pattern in ice age tropical Pacific sea surface temperature. Science 297, 226-230.

Kutzbach, J.E., Wright, H.E., 1985. Simulation of the climate of 18,000 years B.P.: results for the North American/North Atlantic/European sector and comparison with the geological record of North America. Quat. Sci. Rev. 4, 147-187.

Lyle, M., Zahn, R., Prahl, F., Dymond, J., Collier, R., Pisias, N., Suess, E., 1992. Paleoproductivity and carbon burial across the California Current: The Multitraces transect, 42°N. Paleoceanogr. 7, 251-272.

Lyle, M., Koizumi, I., Richter, C., et al., 1997. Proccedings of the Ocean Drilling Program Initial Reports, Vol. 167, Ocean Drilling Program, College Station.

Mangelsdorf, K., Güntner, U., Rullkötter, J., 2000. Climatic and oceanographic variations on the California continental margin during the last 160 kyr. Org. Geochem., 31, 829-846.

Martinson, D.G., Pisias, N.G., Hays, J.D., Imbrie, J., Moore, Jr., T.C., Shackleton, N.J., 1987. Age dating and the orbital theory of the ice ages: Development of a high-resolution 0 to 300,000-year chronostratigraphy. Quat. Res. 27, 1-29.

Meehl, G.A., 1987. The annual cycle and interannual variability in the tropical Pacific

and Indian Ocean regions. Mon. Wea. Rev. 115, 27-50.

Minagawa, M., Winter, D.A., Kaplan, I.R., 1984. Comparison of Kjeldahl and combustion methods for measurement of nitrogen isotope ratios in organic matter. Anal. Chem. 56, 1859-1861.

Morley, J.J., Heusser, L.E., 1997. Role of orbital forcing in east Asian monsoon climates during the last 350 kyr: Evidence from terrestrial and marine climate proxies from core RC14-99. Paleoceanography 12, 483-494.

Mortyn, P.G., Thunell, R.C., Anderson, D.M., Stott, L.D., Le, J., 1996. Sea surface temperature changes in the Southern California Borderlands during the last glacial-interglacial cycles. Paleoceanogr. 11, 415-430.

Moy, C.M., Seltzer, G.O., Rodbell, D.T., Anderson, D.M., 2002. Variability of El Nino/Southern Oscillation activity at millennial timescales during the Holocene epoch. Nature 240, 162-165.

Nakanishi, T., Minagawa, M., 2003. Stable carbon and nitrogen isotopic compositions of sinking particles in the northeast Japan Sea. Geochemical J. 37, 261-275.

Nitta, T., 1987. Convection activities in the tropical western Pacific and their impact on the Northern Hemisphere summer circulation. J. Metor. Soc. Japan 65, 373-390.

Okada, H., McIntyre, A., 1977. Modern cocclithophores of the Pacific and North Atlantic Oceans. Micropaleontology 23, 1-55.

Ortiz, J., Mix, A., Hostetler, S., Kashgarian, M., 1997. The California Current of the last glacial maximum: Reconstruction at 42°N based on multiple proxies. Paleoceanogr. 12, 191-205.

Paillard, D., Labeyrie, L., Yion, P., 1996. Macintosh program performs time-series analysis. EOS Trans. AGU 77, 379.

Pak, D. K., Lea, D. W., Kennett, J. P., 2004. Seasonal and interannual variation in Santa Barbara basin water temperatures observed in sediment trap foraminiferal Mg/Ca. Geochemistry Geophysics Geosystems 5, 12, Q12008, doi:10.1029/2004GC000760.

Petit, J. R., Jouzel, J., Raynaud, D. et al., 1999. Climate and atmospheric history of the past 420,000 years from the Vostok ice core. Nature 399, 429-436. doi:10.1038/20859

Prahl, F.G., Muehlhausen, L.A., Zahnle, D.L., 1988. Further evaluation of long-chain alkenones as indicators of paleoceanographic conditions. Geochim. Cosmochim. Acta 52, 2303-2310.

Prahl, F.G., Paisas, N., Sparrow, M.A., Sabin, A., 1995. Assessment of sea-surface temprature at 42°N in the California Current over the last 30,000 years. Paleoceanogr. 10, 4, 763-773.

Robinson, M.M., 1976. Atlas of the North Pacific Ocean: monthly mean temperature and mean salinities of the surface layer. Reference Publication 2. Naval Oceanographic Office, Washington, D. C.

Sabin, A.L., Pisias, N.G., 1996. Sea surface temperature changes in the northwestern Pacific Ocean during the past 20,000 years and their relationship to climate change in northwestern North America. Quat. Res. 46, 48-61.

Seki, O., Ishiwatari, R., Matsumoto, K., 2002. Millennial climate oscillation in NE Pacific surface waters over the last 82 kyr: New evidence from alkenones. Geophys. Res. Let. 29, 2144, doi:10.1029/2002GL015200.

Stuiver, M., Reimer, P., 1993. Extended ^{14}C database and revised CALIB 3.0 ^{14}C age model calibration program. Radiocarbon 35, 215-230.

Thunell, R.C., Mortyn, P.G., 1995. Glacial climate instability in the Northwest Pacific

Ocean. Nature 376, 504-506.

Yamamoto, M., Yamamuro, M., Tada, R., 2000. Late Quaternary records of organic carbon, calcium carbonate and biomarkers from Site 1016 off Point Conception, California margin. Proc. ODP Sci. Res. 167, 183-194.

Yamamoto, M., Oba, T., Shimamune, J., Ueshima, T., 2004. Orbital-scale anti-phase variation of sea surface temperature in mid-latitude North Pacific margins during the last 145,000 years. Geophys. Res. Let. 31, L16311, doi:10.1029/2004GL020138.

Yamamoto, M., Suemune, R., Oba, T., 2005. Equatorward shift of the subarctic boundary in the northwestern Pacific during the last deglaciation. Geophys. Res. Let. 32, L05609, doi:10.1029/2004GL020138.

Yasunari, T., 1991. “The monsoon year”-A new concept of the climate year in the tropics. Bull. Amer. Meteor, Soc. 72, 1331-1338.

Table captions

Table 1 Age-depth model of ODP Site 1014

Table 2 Age-depth model of ODP Site 1016

Table 1

Depth (mcd)	Method	Conventional age	(±)	Age (years BP)	Reference
0.25	^{14}C of BOM	2830	50	2297	1
1.05	^{14}C of BOM	7800	60	8005	1
1.55	^{14}C of BOM	11310	60	12643	1
1.95	^{14}C of BOM	13240	70	15102	1
2.35	^{14}C of BOM	16450	80	18766	1
2.75	^{14}C of BOM	17150	90	19572	1
3.05	^{14}C of BOM	18000	90	20550	1
Depth (mcd)	OIS			Age (years BP)	Reference
6.20	3.13			43880	2
6.65	3.3			50210	2
7.20	3.31			55450	2
7.45	4			58960	2
8.00	4.22			64090	2
8.70	5			73910	2
9.80	5.1			79250	2
10.55	5.2			90950	2
11.15	5.31			96210	2
11.80	5.33			103290	2
12.55	5.4			110790	2
13.45	5.51			122560	2
13.75	5.5			123820	2
14.05	5.53			125190	2
14.45	6			129840	2
16.75	6.3			142280	2
17.50	6.4			152580	2
18.50	6.41			161340	2

Reference 1: this study, 2: Hendy and Kennett (2000).

Table 2

Depth (mcd)	Method	Conventional age	(±)	Age (years BP)	Reference
0.18	^{14}C of BOM	5550	40	5657	1
0.36	^{14}C of BOM	7900	40	8128	1
0.54	^{14}C of BOM	10950	50	11941	1
0.63	^{14}C of BOM	13130	70	14339	1
0.72	^{14}C of BOM	13480	40	15392	1
0.90	^{14}C of BOM	15090	50	17201	1
1.17	^{14}C of BOM	17400	60	19860	1
1.53	^{14}C of BOM	21380	90	24513	1
1.98	^{14}C of BOM	22950	80	26300	1
2.43	^{14}C of BOM	30440	200	34427	1
2.88	^{14}C of BOM	33660	240	37719	1
Depth (mcd)	Method			Age (years BP)	Reference
3.51	δ^{15}N correlation			48100	1
3.78	δ^{15}N correlation			53545	1
4.50	δ^{15}N correlation			65914	1
5.49	δ^{15}N correlation			75852	1
6.66	δ^{15}N correlation			104290	1
6.93	δ^{15}N correlation			108290	1
7.11	δ^{15}N correlation			112752	1
7.83	δ^{15}N correlation			123274	1
8.46	δ^{15}N correlation			127050	1
8.82	δ^{15}N correlation			133951	1
9.00	δ^{15}N correlation			135573	1

Reference 1: this study.

Figure captions

Fig. 1. Locations of ODP Sites 1014 and 1016 and the California Current System.

Fig. 2. Age–depth models of ODP Sites 1014 and 1016.

Fig. 3. Changes in sedimentary $\delta^{15}N$ and alkenone $U^{K'}_{37}$-derived sea surface temperatures (SSTs) of ODP Sites 1014 and 1016 and the ΔSST_{NEP} ($SST_{ODP1014} - SST_{ODP1016}$) during the last 160 kyr. Data on SSTs for Sites 1014 and 1016 are from Yamamoto et al. (2000, 2004). The calculated NINO3 index (Clement et al., 1999) and the estimated volume of the Laurentide ice sheet (Boulton et al., 1985) are shown for comparison. Blue and green crosses indicate the age controls for Sites 1014 and 1016, respectively, by ^{14}C dating and oxygen isotope stratigraphy.

Fig. 4. The $U^{K'}_{37}$-derived SST, U^{me}_{36}, and $K_{37:4}/K_{37}$ indices for Sites 1014 and 1016 and the abundance of *Coccolithus pelagicus* in relation to total coccoliths at Site 1014. The $\delta^{18}O$ profiles of *Uvigerina* and *Globigerina bulloides* at Site 1014 (Hendy and Kennett, 2000) are shown for comparison. Data for SST, U^{me}_{36}, and $K_{37:4}/K_{37}$ indices at Site 1016, and SST at Site 1014 are from Yamamoto et al. (2000, 2004).

Fig. 5. Plots of $U^{K'}_{37}$–U^{me}_{36} and $U^{K'}_{37}$–$K_{37:4}/K_{37}$ for Sites 1014 and 1016 samples.

Fig. 6. Spectral densities and coherencies of (A) SST versus the $\delta^{18}O$ of *Uvigerina* for Site 1014 at the California margin (3–136 ka, bandwidth = 0.011); (B) the SST of Site 1016 versus the $\delta^{18}O$ of *Uvigerina* in Site 1014, California margin (3–136 ka,

bandwidth = 0.011); (C) ΔSST_{NEP} versus the $\delta^{18}O$ of *Uvigerina* for Site 1014 at the California margin (3–136 ka, bandwidth = 0.011); (D) the SST versus the $\delta^{18}O$ of benthic foraminifera *Uvigerina* for core MD01-2421, Japan margin (5–142 ka, bandwidth = 0.011) and (E) the ΔSST_{NEP} versus the SST in core MD01-2421 (5–136 ka, bandwidth = 0.011). The horizontal dashed line indicates an 80% level of nonzero coherency.

Fig. 7. The $U^{K'}_{37}$-derived SST at the Japan margin (core MD01-2421; Yamamoto et al., 2005), the ΔSST_{NEP} at the California margin and the calculated NINO3 index (Clement et al., 1999) during the last 150 kyr.

Fig. 8. Precession and 30-kyr wheels showing the phases of the SST maxima in core MD01-2421 at the Japan margin, the SST maxima at Sites 1014 and 1016, the ΔSST_{NEP} maxima at the California margin, SPECMAP $\delta^{18}O$ maxima and minima (Imbrie et al., 1984), the predicted NINO3 (Clement et al., 1999), the maximum Indian summer monsoon (summer monsoon stack by Clemens and Prell, 2003), the maximum East Asian summer monsoon (abundance of *Cryptomeria japonica* in core MD01-2421, Igarashi and Oba, 2006), and the maximum primary production in the western equatorial Pacific (Beaufort et al., 2001). Positive and negative angles indicate phase leads and lags, respectively, relative to the precession minima (21 June perihelion) or the pCO_2 maxima.

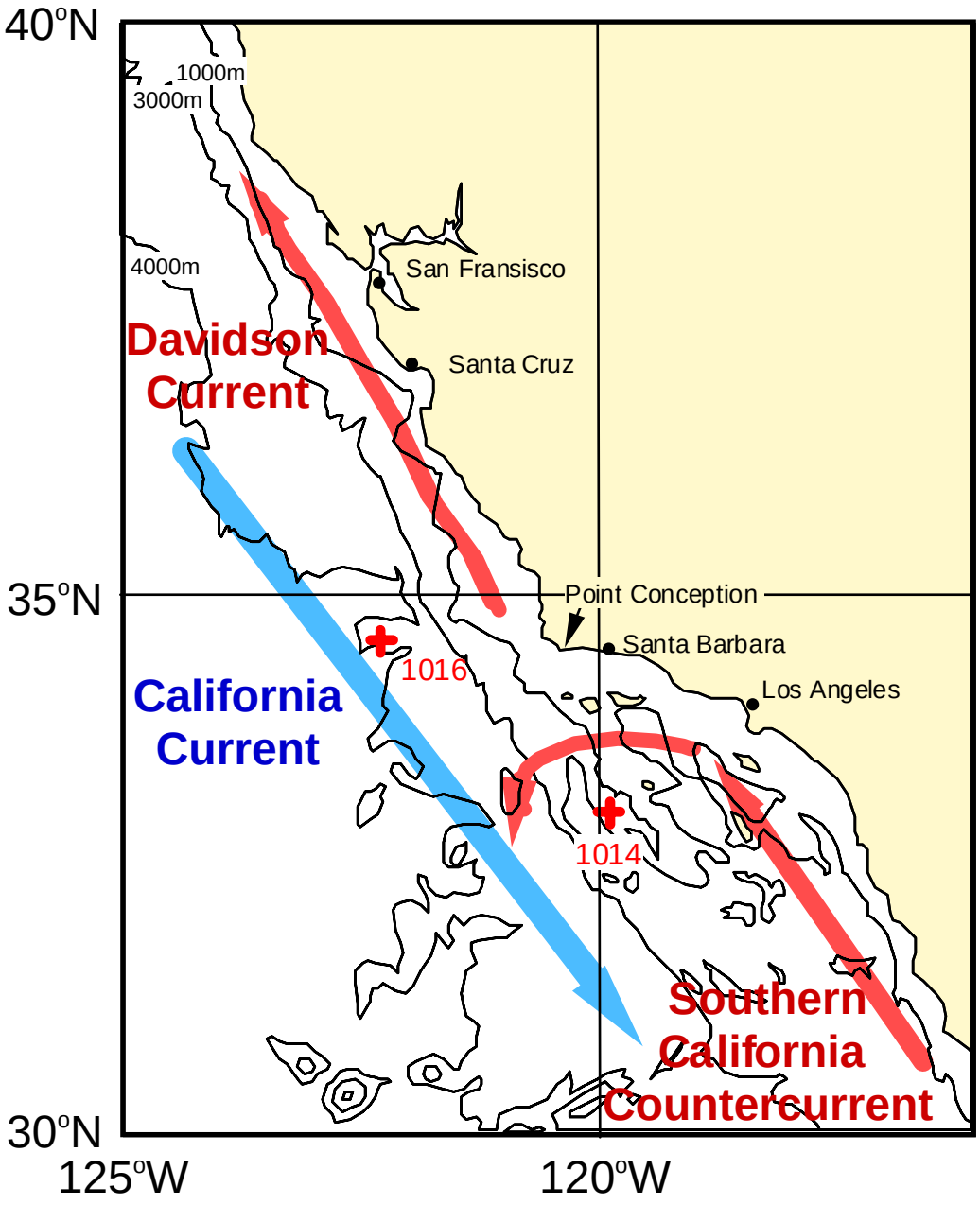
40°N
35°N
30°N
125°W
120°W
1000m
3000m
4000m
San Fransisco
Santa Cruz
Davidson
Current
Point Conception
Santa Barbara
Los Angeles
1016
California
Current
1014
Southern
California
Countercurrent

Fig. 1

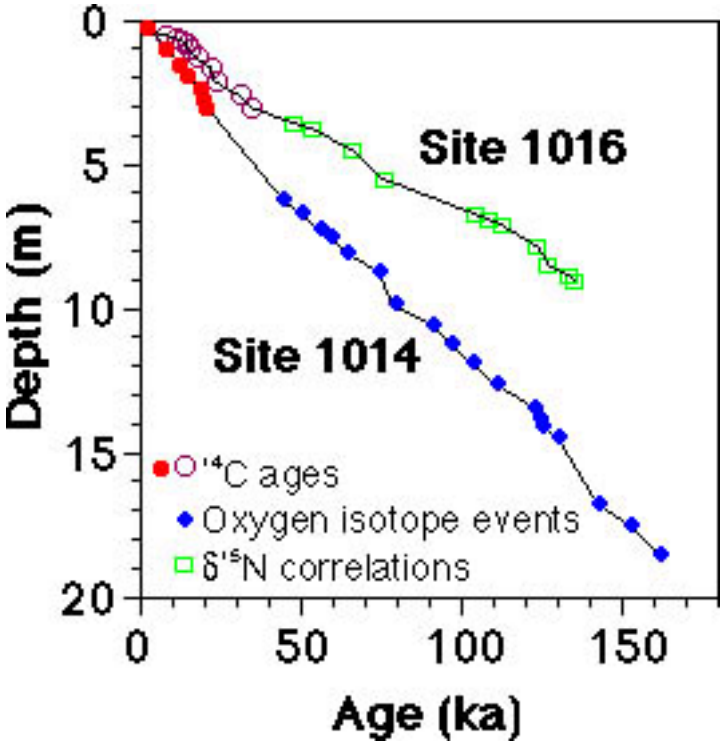
Depth (m)
0
5
10
15
20
0
50
100
150
Age (ka)
Site 1016
Site 1014
^{14}C ages
Oxygen isotope events
δ^{15}N correlations

Fig. 2

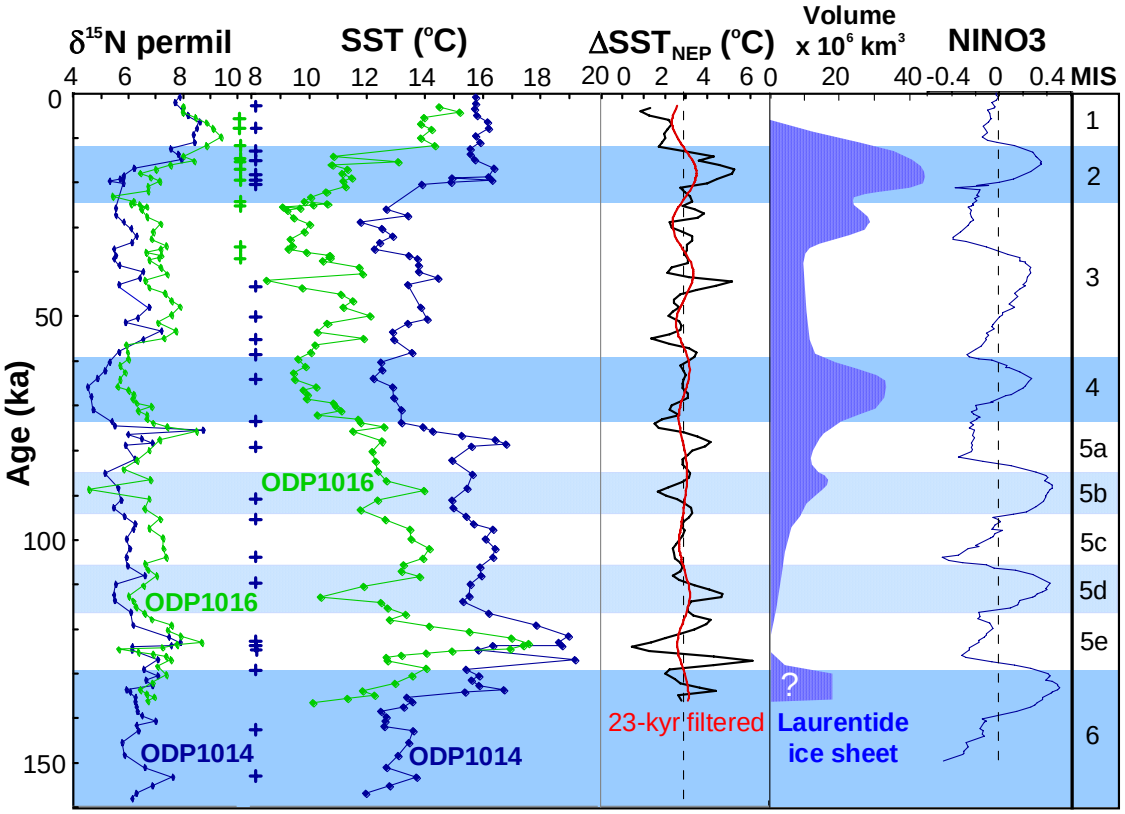
δ15N permil
SST (°C)
ΔSSTNEP (°C)
Volume
x 10⁶ km³
NINO3
MIS
Age (ka)
ODP1016
ODP1016
ODP1014
ODP1014
23-kyr filtered
Laurentide
ice sheet
?

Fig. 3

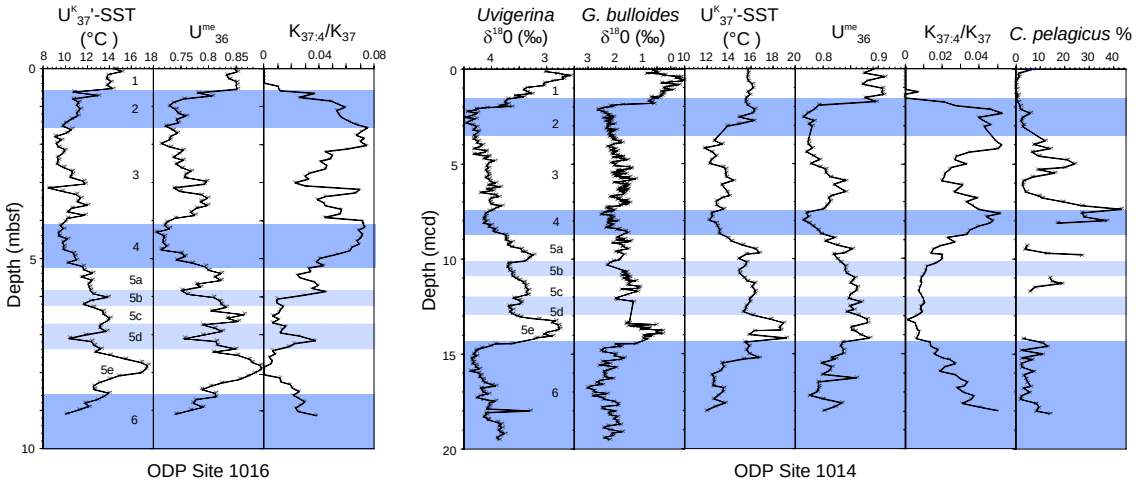
U^K37'-SST (°C)
U^me36
K37:4/K37
Depth (mbsf)
ODP Site 1016
Uvigerina δ18O (‰)
G. bulloides δ18O (‰)
U^K37'-SST (°C)
U^me36
K37:4/K37
C. pelagicus %
Depth (mcd)
ODP Site 1014

Fig. 4

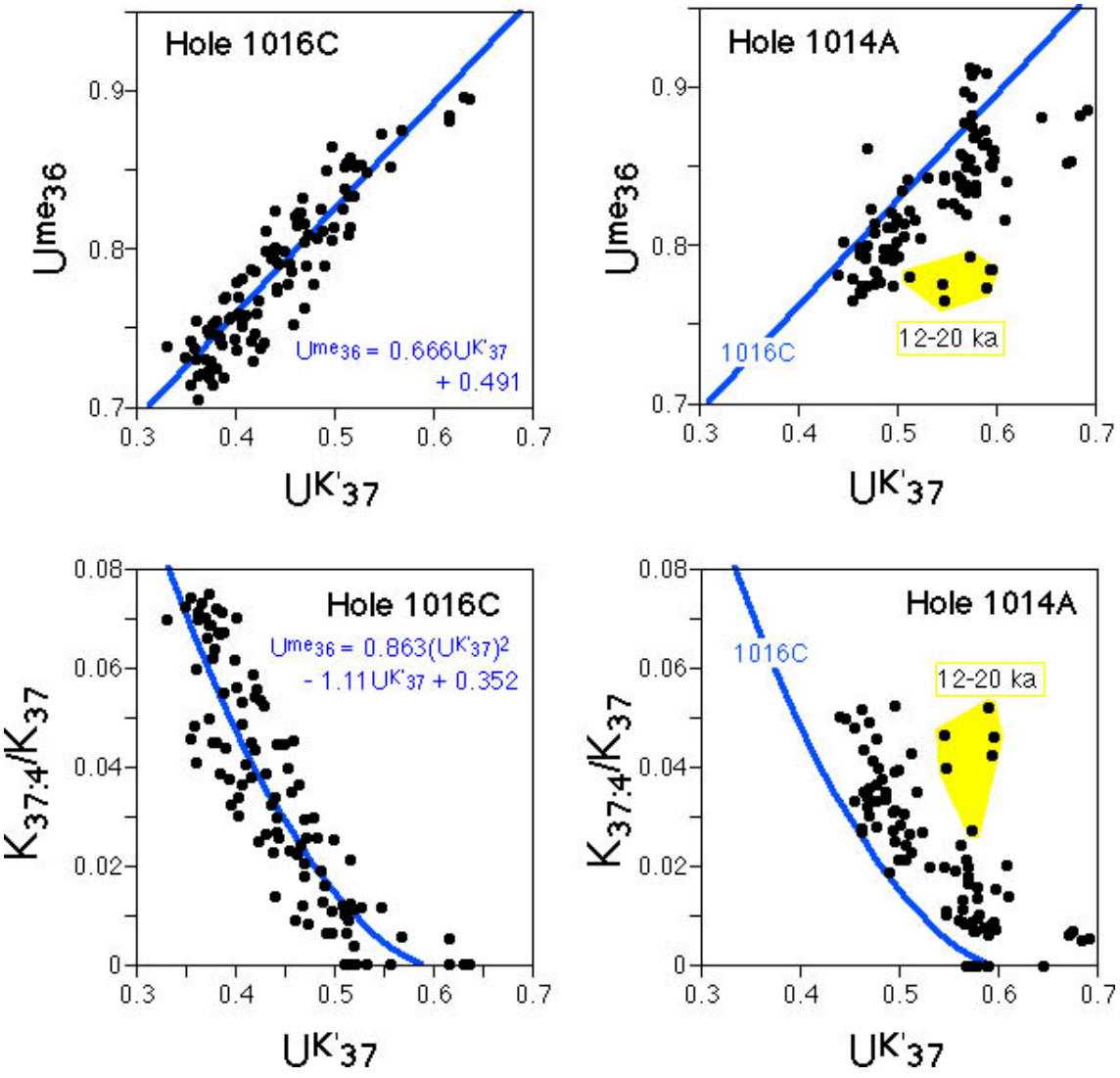
Hole 1016C
Ume36 = 0.666UK'37 + 0.491
Ume36
UK'37
Hole 1014A
1016C
12-20 ka
Ume36
UK'37
Hole 1016C
Ume36 = 0.863(UK'37)2 - 1.11UK'37 + 0.352
K37:4/K37
UK'37
Hole 1014A
1016C
12-20 ka
K37:4/K37
UK'37

Fig. 5

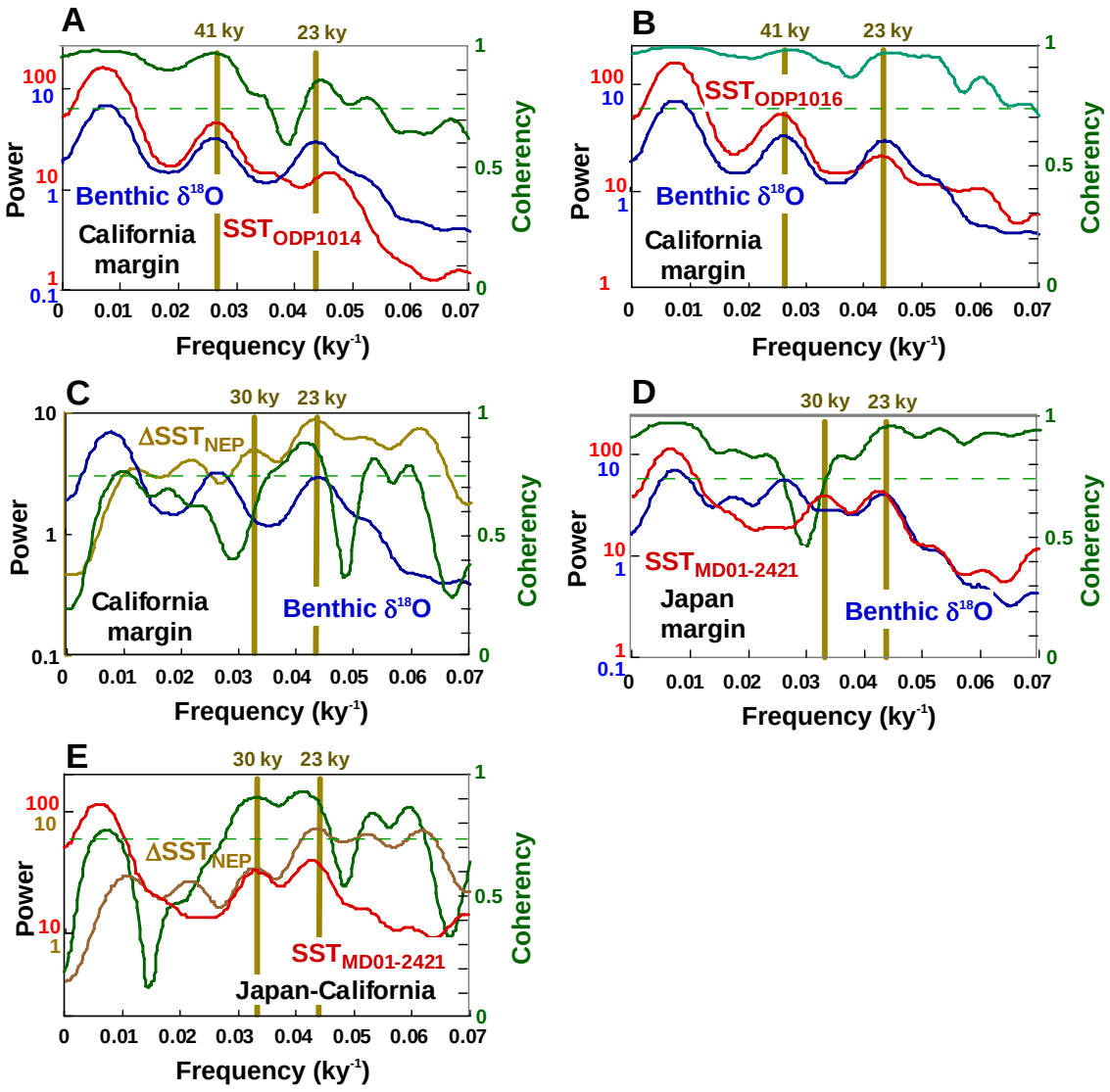
A
41 ky
23 ky
Power
Coherency
Benthic δ18O
California margin
SSTODP1014
Frequency (ky-1)
B
41 ky
23 ky
SSTODP1016
Benthic δ18O
California margin
Frequency (ky-1)
C
30 ky
23 ky
ΔSSTNEP
California margin
Benthic δ18O
Frequency (ky-1)
D
30 ky
23 ky
SSTMD01-2421
Japan margin
Benthic δ18O
Frequency (ky-1)
E
30 ky
23 ky
ΔSSTNEP
SSTMD01-2421
Japan-California
Frequency (ky-1)

Fig. 6

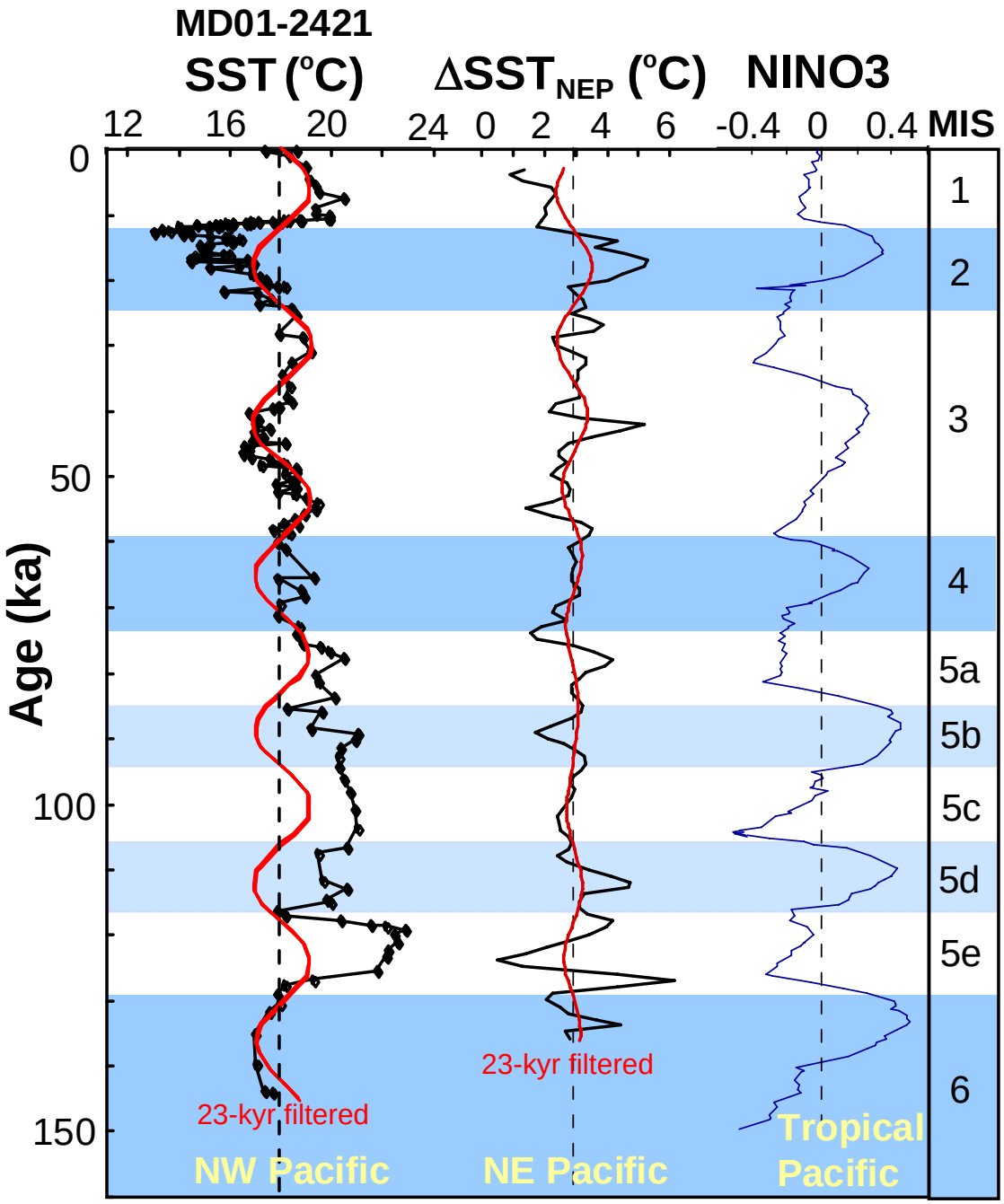
MD01-2421
SST (°C)
ΔSST NEP (°C)
NINO3
12
16
20
24
0
2
4
6
-0.4
0
0.4
MIS
0
50
100
150
Age (ka)
1
2
3
4
5a
5b
5c
5d
5e
6
23-kyr filtered
23-kyr filtered
NW Pacific
NE Pacific
Tropical Pacific

Fig. 7

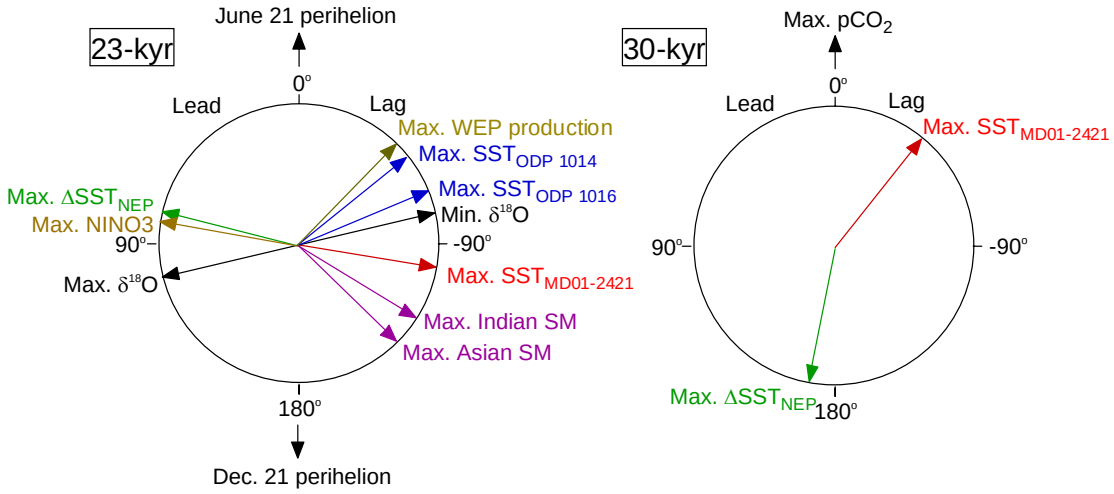
23-kyr
June 21 perihelion
0°
Lead
Lag
Max. WEP production
Max. SST ODP 1014
Max. SST ODP 1016
Min. δ18O
-90°
Max. SST MD01-2421
Max. Indian SM
Max. Asian SM
180°
Dec. 21 perihelion
Max. ΔSST NEP
Max. NINO3
90°
Max. δ18O
30-kyr
Max. pCO2
0°
Lead
Lag
Max. SST MD01-2421
90°
-90°
Max. ΔSST NEP
180°

Fig. 8